Nuclear Inst. and Methods in Physics Research, A 915 (2019) 47–53

Contents lists available at ScienceDirect

Nuclear Inst. and Methods in Physics Research, A

journal homepage: www.elsevier.com/locate/nima

The partial truncated icosahedron phoswich array for detection of low energy charged pions and light charged particles

A. Zarrella [a,b,*], E. Churchman [b,c], J. Gauthier [b], K. Hagel [b], L. Heilborn [a,b], A. Jedele [a,b], Y.-W. Lui [b], A.B. McIntosh [b], A. Rodriguez Manso [b], A. Wakhle [b], M.D. Youngs [b], S.J. Yennello [a,b]

[a] Chemistry Department, Texas A&M University, College Station, TX 77843, USA
[b] Cyclotron Institute, Texas A&M University, College Station, TX 77843, USA
[c] Texas Lutheran University, Seguin, TX 78155, USA

ARTICLE INFO

Keywords:
Phoswich
Pion detection
Pulse shape discrimination

ABSTRACT

The Partial Truncated Icosahedron (ParTI) phoswich array has been designed for the detection of low energy charged pions and other light charged particles for the study of pionic fusion reactions. The array consists of 15 plastic/CsI(Tl) phoswich detector units arranged in approximately one hemisphere of a truncated icosahedron geometry. The phoswich detectors' particle identification capabilities have been characterized. A pulse shape discrimination technique has demonstrated isotopic identification for Z = 1 and Z = 2 particles and elemental identification up to at least Z = 3. Utilization of digital electronics allows for increased sensitivity in event triggering and independent verification of pion detection. A calibration technique for the array has also been developed.

1. Introduction

The ParTI phoswich array was designed for use in an experiment to measure the pionic fusion reaction $^{4}He + {}^{12}C \rightarrow {}^{16}N + \pi^{+}$ for the purpose of identifying charged pions. Pionic fusion is the process by which two nuclei fuse during a collision and then deexcite through the exclusive emission of a pion [1]. The final state consists of a fusion residue which has the same number of nucleons as the reacting system and a pion. The species of the fusion residue and the charge of the emitted pion satisfy charge conservation. The process has been observed in many reacting systems [2–9] with reported reaction cross sections ranging from the order of 100's of nb to 100's of pb for the smallest to largest systems. This extremely coherent process requires that more than 140 MeV of excitation energy from collisions of complex ions is focused into only 2 degrees of freedom — the rest mass and kinetic energy of the emitted pion. These reactions represent the most extreme limit of subthreshold pion production.

Pionic fusion events can be identified through either the detection of the characteristic fusion residue with mass equal to the colliding system and kinetic energy within a well-defined range around the center of mass velocity or through the detection of the emitted pions. An experiment has been designed at the Cyclotron Institute at Texas A&M University which is the first experiment to be sensitive to both the fusion residue and the emitted charged pion. This manuscript will describe the ParTI array which is responsible for the pion detection aspect of the experiment and the complete characterization of its particle identification (PID) and selective triggering techniques.

2. The partial truncated icosahedron (ParTI) phoswich array

In its current configuration, the ParTI phoswich array is comprised of 15 plastic/CsI(Tl) phoswiches arranged on the faces of a truncated icosahedron geometry and covers 19.7% of the solid angle. This results in a detection efficiency of 21.6% for pions produced in the pionic fusion reaction of interest discussed in the previous section. The target is positioned in the center of the truncated icosahedron shape and the distance from the target to the faces of the phoswich detectors is 12.1 cm for pentagonal phoswich geometries and 11.8 cm for hexagonal phoswich geometries (phoswich geometries will be discussed more in Section 2.1). Each face of the array is an individual aluminum frame which holds a single phoswich detector. Those frames are held into the truncated icosahedron shape using aluminum tabs machined to orient the frames at the proper relative angles. A photograph of the populated ParTI array is shown in Fig. 1. Because each detector frame is an independent part, the array geometry can be changed for different experimental needs. The ParTI phoswiches can be used in various configurations including a wall or ring by machining appropriate tabs and different portions of the truncated icosahedron geometry can be accessed with existing parts.

* Corresponding author at: Cyclotron Institute, Texas A&M University, College Station, TX 77843, USA.
E-mail address: azarrella@comp.tamu.edu (A. Zarrella).

https://doi.org/10.1016/j.nima.2018.10.161
Received 18 June 2018; Received in revised form 6 September 2018; Accepted 21 October 2018
Available online 26 October 2018

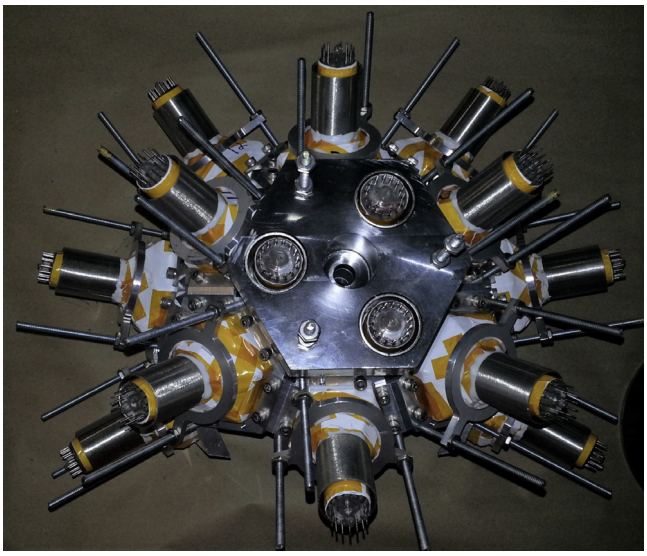

Fig. 1. A photograph of the populated ParTI phoswich array viewed from the upstream side. (color online).

2.1. The ParTI phoswiches

The ParTI phoswiches are composed of a layer of EJ-212 fast-scintillating plastic and a layer of CsI(Tl) that are optically coupled together and to a single photomultiplier tube (PMT). The array uses 3 different phoswich geometries. Of the 15 total phoswiches in the current construction, 12 have geometries of regular pentagons or hexagons which correspond to the faces of the truncated icosahedron shape. Each side of the regular polygons is 3.8 cm. The 3 other phoswiches are modified hexagonal geometries such that the three detectors fit in a special hexagonal frame with a hole in the center for the beam to pass through. This can be seen at the center of the array in Fig. 1.

Regardless of the geometry, each of the phoswiches has the same component construction. The front face of the detectors is a 3 mm thick layer of EJ-212 which was chosen for its fast rise and decay times (0.9 ns and 2.4 ns, respectively). The next component is a 1.5 cm thick layer of CsI(Tl). The CsI(Tl) scintillation has two prominent components (600 ns and 1 μs), both of which are much slower than the fast plastic which results in a response that can be separated from the plastic response. Following the CsI(Tl) crystal is a 2.54 cm thick Lucite light guide which couples the polygonal shape of the scintillating components to the circular face of a 1924a Hamamatsu PMT. The plastic/CsI(Tl) and CsI(Tl)/light guide couplings are made with a thin layer of BC-630 optical grease. The light guide/PMT coupling is made using RTV-615 optical adhesive. The front face of each phoswich is covered with a layer of 420 μg/cm^2 aluminized Mylar® to provide a uniformly thin and reflective barrier. All other faces of the phoswiches are wrapped with white teflon tape and no Mylar. Fig. 2 is a photograph of two completed phoswiches, one pentagonal geometry and one hexagonal.

3. Fast vs. slow particle identification and calibration method

The selection of two scintillating components with very different decay characteristics allows for a fast vs. slow pulse shape discrimination (PSD) method in order to achieve PID. The ParTI phoswiches were simulated using Geant4 [10] in order to predict their PID capabilities. In each Geant4 phoswich event a single particle is fired into the front face of the simulated detector. The identity of the particle was selected at random from 10 possible species: neutron, γ, proton, deuteron, triton, ^{3}He, α, ^{6}Li, π^+, π^-. The range of simulated particle energies varies by particle type. For protons, deuterons, and tritons the energy range is from E_{min} = 5 MeV to E_{max} = 70 MeV, 90 MeV and 110 MeV, respectively. For tritons, ^{3}He, α, and ^{6}Li events the energy range is from E_{min} = 5 MeV to $E_{max} = 2 * Z * 60$ MeV where Z is the particle's proton number. The charged pion energies range from E_{min} = 5 MeV to $E_{max} = E^*_{PF}$, the energy above the pionic fusion threshold for the pionic fusion experiment mentioned in Section 1. Lastly, the angle of trajectory with respect to the face of the detector was randomized on an event-by-event basis with a maximum simulated angle corresponding to the distance from the center of the phoswich to the corners. This accounts for the range of possible energy losses due to the different effective thicknesses of the phoswich components as a function of incident angle. An example of a Geant4 simulated phoswich response to an incident alpha particle is shown in Fig. 3. The vertical axis is the count of photons reaching the PMT face and the horizontal axis is the time since the arrival of the first photon at the PMT in ns.

The PSD is accomplished by integrating the waveform response inside two time regions, one corresponding to the scintillation response of the fast plastic and the other corresponding to the scintillation of the CsI(Tl) component. The fast integration region starts at the beginning of the simulated response and spans 28 ns. The fast integration window is shown in Fig. 3 as the red shaded region and encompasses the sharp peak produced by the fast plastic response. The slow integration region begins 48 ns after the start of the phoswich response and spans 400 ns. The slow integration window is shown as the green shaded region in Fig. 3. The widths and locations of these integration regions were determined by investigating many configurations of the gates in the Geant4 simulation and comparing the PID quality at each iteration.

The two integrations can be used to produce the fast vs. slow PID plot shown in Fig. 4. The horizontal axis is the photon sum inside the slow integration gate and the vertical axis is the photon sum inside the fast integration gate. The different color points correspond to different particle types — blue for neutrons, green for γs, red for charged pions, and black for the other light charged particles which are labeled next to their respective lines. The neutron and γ responses largely lie on top of each other to form the neutron/γ line. The charged pion PID line contains events from both π^+ and π^- primary events. These events are clearly separated from the neutron/γ line below and from the proton line above. Thus, Geant4 predicts that the ParTI phoswiches will be sensitive to charged pions and capable of efficiently identifying them. Furthermore, the simulation indicates that if one records the entire phoswich response waveform, there is a second charged pion identification method that can be utilized for π^+ primary events.

After implantation in the detector material (or possibly in flight on the way to the detector), the π^+ particle with a mean lifetime of 26 ns will decay into a $\mu^+ + \nu_\mu$. This 2-body decay results in 4.12 MeV of kinetic energy for the μ^+. The phoswich response to this decay is difficult to separate from the implantation response, however, since it follows so shortly after the implantation. The μ^+ is likely to have also stopped in the detector material (unless it was produced close to an outside wall of the detector) and will subsequently decay into $e^+ + \nu_e + \bar{\nu_\mu}$ with a mean lifetime of 2.2 μs. This will produce a scintillation response from the stopping of the e^+. Since it is a 3-body decay, the positron will have a distribution of possible kinetic energies which is peaked around 50 MeV [11]. These positrons have enough energy that they are likely to leave the detector before completely stopping. The energy deposited on their way out and their longer mean lifetime compared to the scintillation components of the phoswich, though, make the resulting phoswich response identifiable.

Fig. 5 shows an example of one of these π^+ primary events simulated in Geant4. Unlike in the waveform in Fig. 3, there is a second peak from the μ^+ decay which is clearly visible. A second method of identification for π^+ events can be established using this characteristic shape of the phoswich response. This method cannot be efficiently used to identify π^- primary events as the capture lifetime of the μ^- on the nuclei in the detector material is much shorter than the decay lifetime [12].

Experimentally, each phoswich response is digitized and recorded using the Struck Innovative Systeme (SIS) 3316 VME digitizer with 250 MHz sampling rate. With access to the experimental waveform responses, the same analysis as described above can be performed on the experimental data.

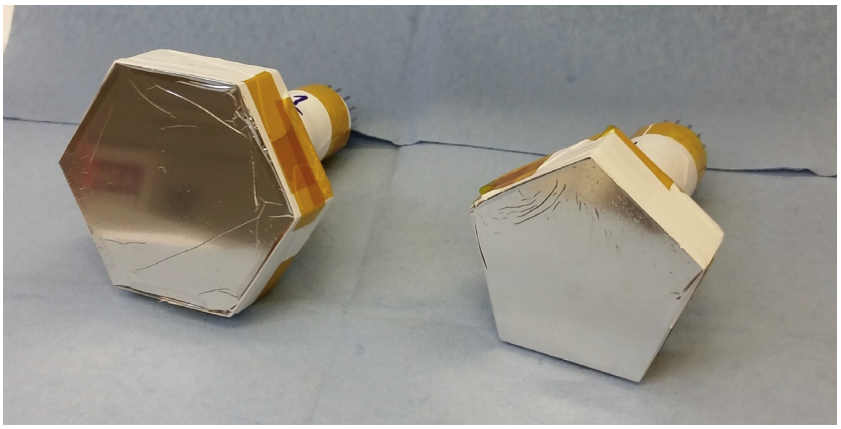

Fig. 2. A photograph of two ParTI phoswiches outside of the array. (color online).

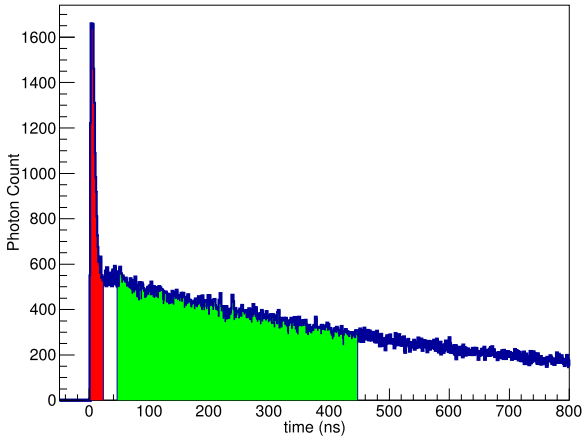

Fig. 3. A Geant4-simulated phoswich response to an incident alpha particle. The vertical axis is the number of collected photons and the horizontal axis is time since first photon arrival in ns. The red shaded region corresponds to the fast integration window and the green shaded region corresponds to the slow integration region . (For interpretation of the references to color in this figure legend, the reader is referred to the web version of this article.)

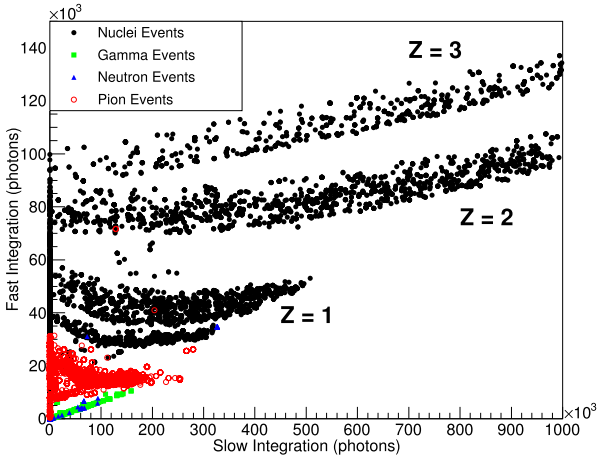

Fig. 4. The fast vs. slow PID figure produced by the Geant4 simulation of phoswich responses to neutrons, γs, and light charged particles. The vertical axis is the integrated photon count inside the fast gate and the horizontal axis is the integrated photon count inside the slow gate. The phoswich responses to different particle types are shown in the various colors (online) and marker styles — blue triangles for neutrons, green squares for γs, red open circles for charged pions, and black closed circles for other light charged particles whose proton numbers are noted next to each line.

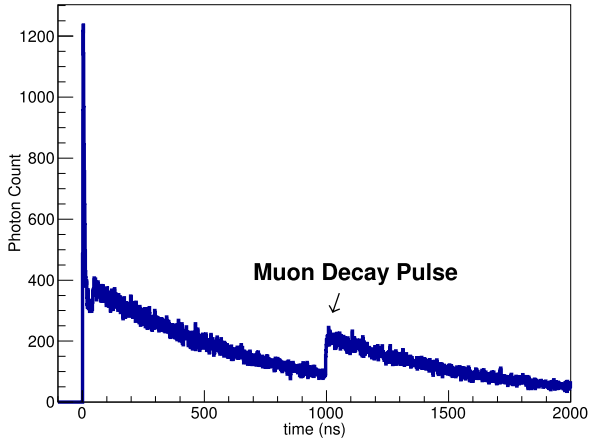

Fig. 5. An example Geant phoswich response waveform created by an incident π^+ particle. The vertical axis is the number of photons collected and the horizontal axis is the time since first photon arrival in ns. The second pulse is the detector response to the μ^+ daughter's decay and its presence in the waveform can be used to identify the π^+ primary.

3.1. PID and calibration using secondary beams

For the purposes of characterizing and calibrating the ParTI phoswiches, a beam of ^{16}O was accelerated to 3.9 MeV/nucleon by the K500 superconducting cyclotron at Texas A&M University and impinged on a ^{9}Be production target. The Momentum Achromat Recoil Spectrometer (MARS) [13] was used to separate and focus secondary beams of known species and energy onto ParTI phoswiches which were mounted at the spectrometer focal plane. The data can then be used to create a calibration template for the phoswiches. In experiments for which calibration cannot be done using radioactive sources or calibration beams, these calibration templates can be used to perform a successful calibration.

Fig. 6(a) is the fast vs. slow PID figure for a hexagonal geometry phoswich produced using a compliment of secondary beams from MARS. The vertical axis is the integration of digitized ADC channels inside the fast gate and the horizontal axis is the integration inside the slow gate. The spectrometer was focused on the N = Z particle line for 5 magnetic rigidity settings. From bottom to top, one can see the neutron/γ line extending out from approximately (0,0). Next is a band corresponding to protons which are uncorrelated with the spectrometer settings as they are primarily produced in reactions on the MARS slits located directly in front of the focal plane chamber. The proton band is followed by a series of 5 spots which are the phoswich responses to the 5 energies of deuteron secondary beams with magnetic rigidities ($B\rho$) = 1.0 Tm, 1.2 Tm, 1.3

Tm, 1.4 Tm, and 1.5 Tm. Above the deuterons are 4 spots which are a result of alpha secondary beams at the 4 highest $B\rho$ settings mentioned above (the lowest energy alpha beam does not punch through the plastic layer). Lastly, there are two spots above the alphas which correspond to two energies of ^{6}Li secondary beams at the two highest $B\rho$ settings (^{6}Li at the lower rigidity settings stop in the plastic layer). Spanning the entire vertical range to the left of the data is the "punch-in" line which is populated by charged particle events in the phoswiches that stop in the fast plastic and do not punch into the CsI(Tl) layer.

The process for creating the ParTI phoswich calibration templates generally follows the technique discussed in Ref. [14]. The first step of the method is correcting for the shapes of the punch-in and neutron/γ lines. Incident neutrons and γs which populate the line are only depositing energy in the CsI(Tl) layer of the phoswich. Because no energy is deposited in the fast plastic, the neutron/γ line should lie on the horizontal axis in ΔE-E PID space. In fast vs. slow space, though, it is clearly sloped. This is due to the fact that, despite its relatively slow rise time, the CsI(Tl) scintillation begins at the moment of the charged particle interaction. Thus, there is some non-zero integration of the CsI(Tl) response inside the fast integration gate. Similarly, the punch-in line corresponds to particles stopping inside the fast plastic and depositing no energy inside the CsI(Tl) layer and yet the responses do have some slow integration due to the fast scintillation "leaking" into the slow gate in the same way. In order to move forward with the energy calibration, these contributions must be corrected for. Also, the intersection of these two lines represent (0,0) in energy space but are shifted in fast vs. slow space due to statistical fluctuations in the waveform's baseline event-by-event.

The two red lines in Fig. 6a represent polynomial fits of the punch-in (second order) and neutron/γ (first order) lines. These two fits are used to correct the fast and slow integrations of the waveforms event-by-event using Eqs. (1) and (2) where F and S refer to the fast and slow integrations, (S_{int}, F_{int}) is the intersection point of the two fits, and $M_{n/\gamma}$ is the slope of the neutron/γ line fit. The values of a_1 and a_2 are the coefficients from the second order fit of the punch-in line after the fast vs. slow space has been inverted to produce a fit of slow integration as a function of fast integration.

$$F' = (F - F_{int}) - (S - S_{int})M_{n\gamma} \tag{1}$$

$$S' = (S - S_{int}) - (F - F_{int})^2 a_2 - (F - F_{int})a_1 \tag{2}$$

The corrected fast vs. slow PID space is shown in Fig. 6b where the neutron/γ line is now on the horizontal axis and the punch-in line is on the vertical axis. This corrected fast vs. slow PID figure (and a figure produced through the same process for a pentagonal geometry) is the calibration template that can be used to calibrate the ParTI phoswiches in future experiments. In those cases, the raw fast vs. slows should be corrected for the shapes of the punch-in and neutron/γ lines and the location of the intersection in the same way that was done above. Then, the fast and slow integrations should be scaled such that they match the appropriate template. The scaling process accounts for gain differences between experiments arising from different PMT biases or intrinsic gain differences between PMTs.

Energy calibrations are produced for both the energy deposited in the fast plastic and the CsI(Tl) crystal from the fast vs. slow template in Fig. 6b. These energy calibrations can be used for any future phoswich data which has been corrected and properly scaled to match the template.

4. Characterization of the ParTI phoswich response to π^+

Three ParTI phoswiches (2 hexagonal and 1 pentagonal) were transported to the Paul Scherrer Institute (PSI) in Switzerland where the detector responses to π^+ implantations were studied. The experiment was performed in the πM1 beam line and copper degraders were used to degrade the pion beams to access the energy range of interest for pionic fusion reactions, approximately 5 MeV to 30 MeV. Fig. 7a shows the fast vs. slow PID figure for the π^+ data collected in a representative phoswich at PSI along with a set of proton/deuteron reference beams also taken at PSI. The charged pion, proton, and deuteron PID lines are labeled. The pion PID line is clearly separated from the proton and neutron/γ lines. The pion line is also populated with the μ^+ daughters of pions that have decayed in flight on the way to the phoswiches. The resolution of the detectors is not sufficient, though, to separate the two particles as their masses only differ by approximately 35 MeV and their charges are equal. This ambiguity does not affect the any of the results of the following analyses, however, and this PID line will continue to be referred to as the pion PID line.

Like before, the vertical axis in Fig. 7a is the integration of the phoswich response waveform inside the fast gate in ADC channels and the horizontal axis is the integration inside the slow gate. Panel (b) of Fig. 7 shows a closer look at the pion PID line from panel (a) with the software PID gate for pions (solid) and a gated background region (dashed) overlaid. The characteristics of the events inside the two gated regions can help further characterize the phoswich responses to π^+ implantations.

While the π^+ beam data in both panels of Fig. 7 were being collected, the data acquisition was employing a "muon decay trigger". When implemented, a trigger is produced by the SIS3316 digitizer upon the second instance of the signal passing threshold within a digitization window. This trigger was developed in order to facilitate the measurement of very low probability pion production reactions (in this case, pionic fusion) by selectively triggering on pion primary events. Phoswich responses to π^+ events are likely to pass the trigger conditions due to the second pulse produced by the muon daughter's decay while all other particle interactions do not have this characteristic waveform shape.

4.1. π^+ waveform analysis

As mentioned above, the characteristic phoswich response due to pion implantations that are followed by decays of the muon daughters can be used to distinguish pion events from other charged particles. Fig. 8 shows one of the digitized phoswich responses for an event that falls inside the pion PID gate in Fig. 7b. The vertical axis is the ADC value in channels and on the horizontal axis is time since the start of the digitization window in ns. The sharp peak followed by the slow decay is the phoswich response to the charged particle implantation and the second pulse with the slower rise around 8000 ns is due to the daughter muon's decay inside the CsI(Tl) layer.

The time between the initial implantation of the pion into the detector and the muon-like decay pulse is defined as Δt. Because Δt varies from decay to decay, the time locations of the two pulses have to be determined event-by-event. Because the charged particle implantation always begins with a sharp rise from a clean baseline, the time associated with the implantation is considered to be the first bin of the digitized response that is above a software threshold. The decay pulse, however, is more difficult to locate because the rise is typically more gradual and it is often riding along the fall from the implantation response so there is not a good baseline. Fortunately, because the muon decay trigger is selecting that second pulse, the time associated with the decay pulse can be approximated to be the location of the trigger within the digitization window which is constant for all events.

The distributions of Δt for events inside the pion PID gate are shown for each of the three phoswiches in the PSI experiment in the left column of Fig. 9. The right column shows the Δt distribution for events inside the gated background regions for the three phoswiches. Each one of the histograms is a measurement of the decay curve associated with the incident particle species (or, possibly, multiple particle species) inside of the PID line or background area. Beyond the requirement that all analyzed events must have produced detector responses that meet the

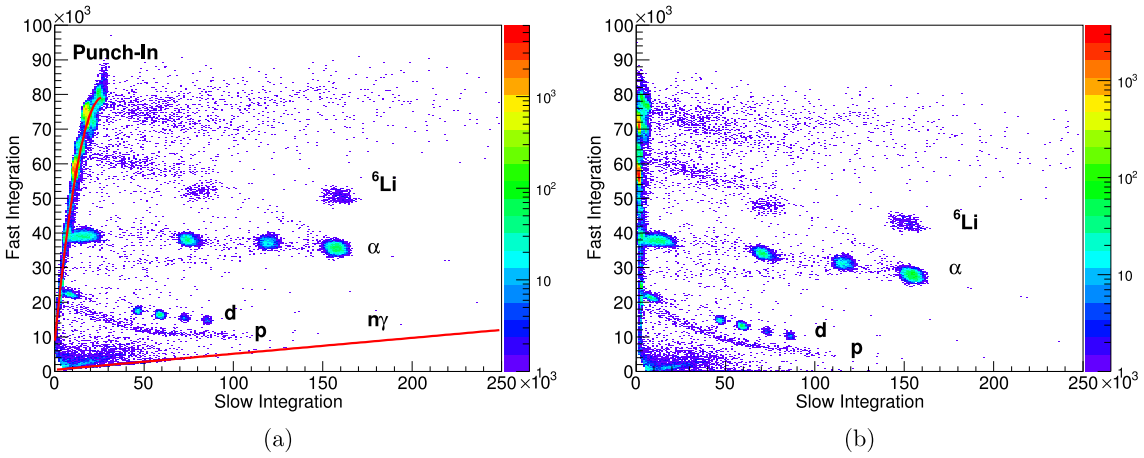

Fig. 6. (a) The fast vs. slow PID figure from a hexagonal geometry phoswich exposed to secondary beams at the focal plane of MARS. The vertical axis is the integration of waveform response inside the fast gate in ADC channels and the horizontal axis is the integration inside of the slow gate. The red curves are fits of the punch-in and neutron/γ lines and each PID band is labeled with the corresponding PID. (b) The same fast vs. slow phoswich data from panel (a) after the correction for the punch-in and neutron/γ lines has been made. (color online).

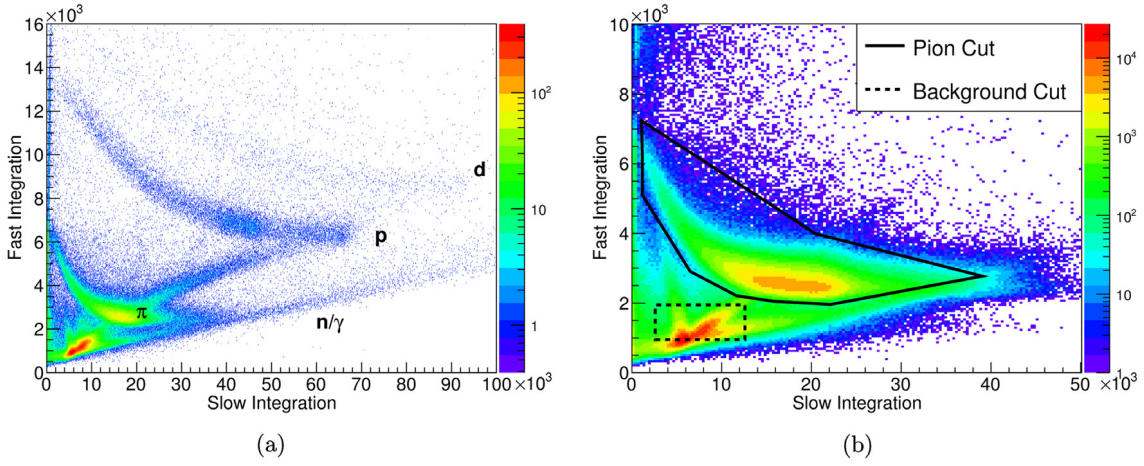

Fig. 7. (a) The fast vs. slow PID figure from a representative ParTI phoswich during the PSI experiment. The vertical axis is the integration of the waveform response inside the fast gate in ADC channels and the horizontal axis is the integration inside of the slow gate. The PID lines corresponding to the neutron/γ line and the phoswich responses to π^+, proton, and deuteron implantations are labeled in the figure. (b) A closer look at the π^+ PID line from panel (a). The software PID gates for pions (solid) and a gated background region (dashed) are overlaid. This figure does not include any data collected during the proton/deuteron beam runs. (color online).

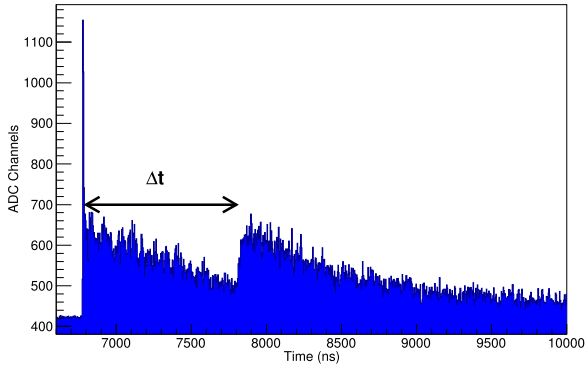

Fig. 8. An experimental waveform for an event whose fast and slow integrations fall inside of the pion PID gate in Fig. 7b. The vertical axis is the ADC value in channels and the horizontal axis is the time since the beginning of the digitization window in ns. The sharp peak followed by the slow decay toward baseline is the phoswich response to the charged pion implantation and the second, slower rising pulse is the response to the daughter muon's decay inside the CsI(Tl) crystal. The time between the implantation and the decay is defined as Δt. (color online).

muon decay trigger criteria, all events in this analysis have a Δt of at least 1000 ns. By not considering the lower region of the Δt distributions, we can be confident that the measured fast and slow integrations of the implantation pulses are not contaminated by the decay-like pulses. Also, this eliminates cases where statistical fluctuations in the implantation response satisfy the muon decay trigger prematurely.

For each of the decay curves in Fig. 9, an exponential fit of the form of Eq. (3) can be implemented. Here, the exponential term, λ, is the decay constant of the particles inside the gated region and the constant offset, a_0, is allowing for a flat background. The red curves overlaid in Fig. 9 represent these fits for the pion-gated data in each of the ParTI phoswiches. In each pion-gated panel, next to each fit line is the value of τ extracted from the fit of the decay curve where $\tau = 1/\lambda$.

$$N = N_0 e^{-\lambda dt} + a_0 \tag{3}$$

It is clear from the comparison of the pion-gated data to the gated background data that the particles populating the pion PID line are decaying after implantation and that those particles populating the background region are not showing any obvious decays which is the expectation if the events populating this region are from random coincidences. The mean lifetimes calculated from the decay constants in Fig. 9 are all within 1% of the known value for τ_{μ^+}, 2197 ns.

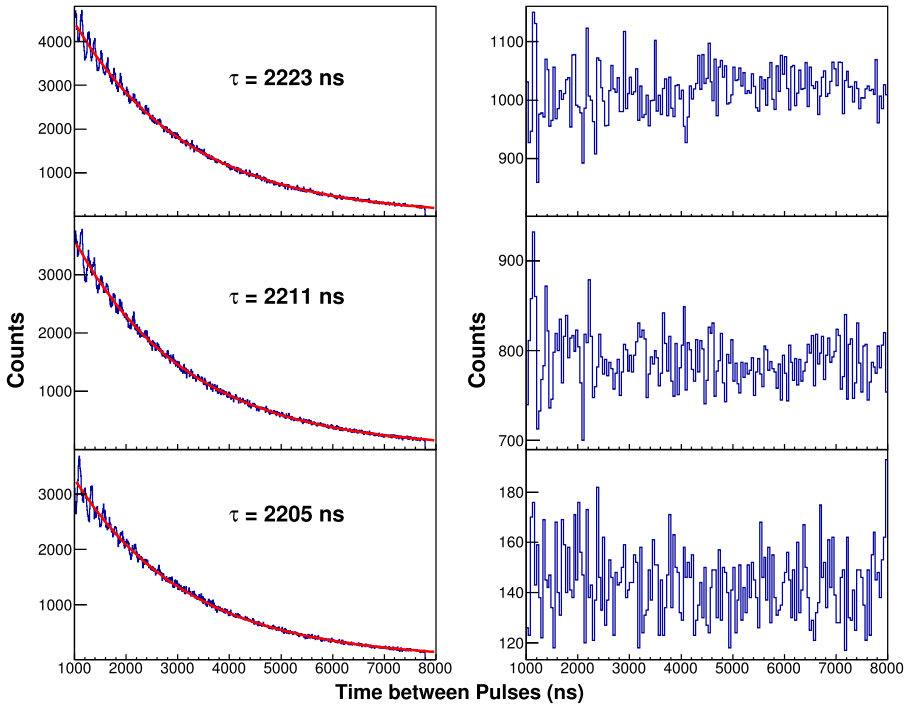

Fig. 9. (Left column) Decay curves for events inside of the pion PID gates for each of the three phoswiches with the exponential fits of the form of Eq. (3) overlaid in red. The extracted mean lifetime, τ, from each of the fits is given in all 3 cases. (Right column) The same Δt analysis for events inside the gated background regions for the 3 ParTI phoswiches. (color online).

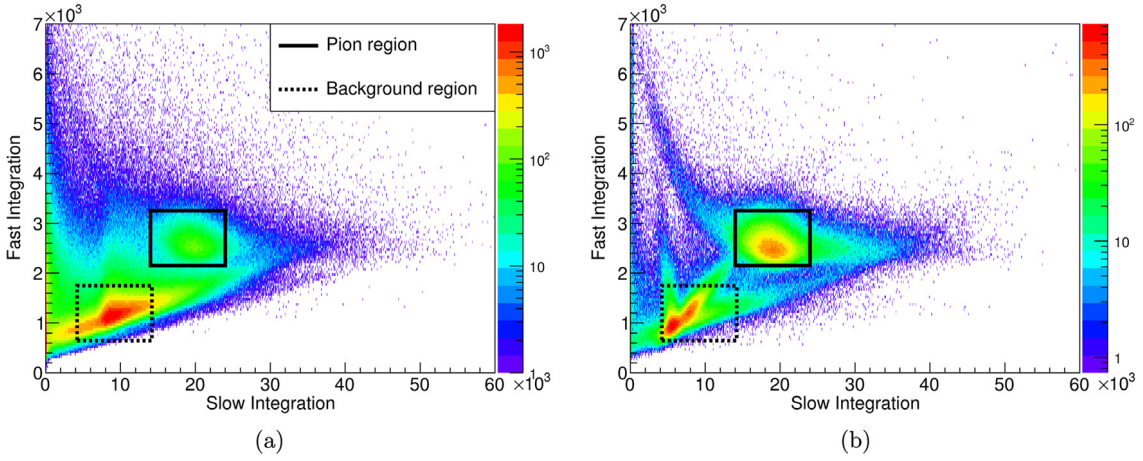

Fig. 10. (a) A representative fast vs. slow PID figure for data collected with a π^+ beam while the SIS3316 digitizer's standard trigger was implemented. (b) The fast vs. slow PID figure for the same phoswich and same beam as panel (a) but with the muon decay trigger implemented. A gated region inside the pion PID area (solid) and a gated region in a background region (dashed) are overlaid in both figures. (color online).

4.2. The effect of the muon decay trigger

As previously mentioned, the muon decay trigger was developed in order to increase the ParTI array's sensitivity to pion-like events. During the pionic fusion experiment, the array is located inside the target chamber and, consequently, the phoswiches are subjected to a high rate of background. With a standard triggering scheme, the acquisition would be swamped by these uninteresting events resulting in an unacceptable dead time for the measurement of low cross section reactions. The effect of the muon decay trigger on pion event sensitivity is shown in Fig. 10.

In both panels of Fig. 10 the vertical axis is the integration of the phoswich response inside the fast gate and the horizontal axis is the integration inside the slow gate. The data shown was collected by the same phoswich in the PSI experiment and for the same π^+ beam. In panel (a) the acquisition is being triggered using the SIS3316's standard CFD triggering functionality and in panel (b) the muon decay trigger is implemented.

Immediately, it is clear that the muon decay trigger has significantly increased the pion sensitivity as the ratio of the population in the pion line to all other background events has increased. In order to quantify the effect, two software gates are created and shown overlaid in the two figures. The size of the solid-lined gate was chosen as to encompass the primary region corresponding to the pion beam spot in Fig. 10b. The dashed-lined gate surrounds a region populated by background events. Both gates are the same size and their size and positions do not change between panels. A ratio of the number of events inside the two gates shows that the muon decay trigger has increased the pion selectivity by approximately a factor of 10. This result should be considered a proof of the muon decay trigger's usefulness, not an expectation to be applied

to future experiments. The increased selectivity that can be obtained using the muon decay trigger is dependent upon the type and rate of background particle implantations as well as hardware thresholds and the amount of noise in the electronics.

5. Conclusion

The ParTI array has been designed for the detection of charged pions and other light charged particles resulting from pionic fusion experiments. The plastic/CsI(Tl) phoswiches have been constructed and have been shown to have good PID capabilities for pions and light charged particles using fast vs. slow PSD. The SIS3316 digitizers have been used to record phoswich response waveforms which have been shown to be able to aid in the detection of pion events using the characteristic shape produced by the decay of daughter muons. The muon decay trigger which was developed for the pionic fusion experiment is working as intended with the ability to increase sensitivity to pion-like events by at least an order of magnitude. The results reported here indicate that the ParTI array meets the necessary criteria for use in the pionic fusion experiments for which it was designed. It has the potential to also be useful for a range of experiments which require a flexible array with large angular coverage for the detection of light charged particles.

Acknowledgments

This work was supported by the Robert A. Welch Foundation, USA [Grant A-1266] and the U.S. Department of Energy DOE, USA [Grant DE-FG02-93ER40773]. We would like to thank the excellent staff at the Texas A&M University Cyclotron Institute for providing the experimental beams and technical support. We would also like to thank the Paul Scherrer Institute for providing us with beam time and, especially, the PSI πM1 beam line group for making the experiment possible.

References

[1] P. Braun-Munzinger, J. Stachel, Pion production in heavy-ion collisions, Annu. Rev. Nucl. Part. Sci. 37 (1987) 97–131.
[2] D. Horn, et al., Pionic fusion of heavy ions, Phys. Rev. Lett. 77 (1996) 2408–2411.
[3] Y. Le Bornec, et al., Coherent pion production near threshold with a ^{3}He projectile, Phys. Rev. Lett. 47 (1981) 26–30.
[4] L. Joulaeizadeh, et al., Pionic fusion in light-ion systems, Phys. Lett. B 694 (2011) 310–315.
[5] W. Schott, et al., Observation of the^{12}C(^{3}He, π^{+})^{15}N reaction near threshold using recoil detection, Phys. Rev. C 34 (1986) 1406–1410.
[6] M. Andersson, et al., Pionic fusion study of the ^{6}He halo, Nuclear Phys. A 779 (2006) 47–62.
[7] L. Bimbot, et al., Experimental study of coherent pion production in ^{4}He(^{3}He, π^{+})^{7}Li and a test of the reaction mechanism, Phys. Lett. B 114 (1982) 311–314.
[8] J. Homolka, et al., Measurement of the^{12}C(^{3}He, π^{+})^{15}N reaction cross section near threshold, Phys. Rev. C 38 (1988) 2686–2691.
[9] N. Willis, et al., Coherent pion production in ^{6}Li(^{3}He, π^{+})^{9}B and^{10}B(^{3}He, π^{+})^{13}C close to threshold, Phys. Lett. 136 (1984) 334–336.
[10] S. Agostinelli, et al., GEANT4 - a simulation toolkit, Nucl. Instrum. Methods A 506 (2003) 250–303.
[11] J. Barlow, et al., The momentum spectrum of electrons from muon decay, Proc. Phys. Soc. 84 (1964) 239–244.
[12] A. Grossheim, et al., Decay of negative muons bound in^{27}Al, Phys. Rev. D 80 (2009) 053001.
[13] R.E. Tribble, R.H. Burch, C.A. Gagliardi, MARS: A momentum achromat recoil spectrometer, Nucl. Instrum. Methods A 285 (1989) 441–446.
[14] D.A. Cebra, et al., The light response of plastic scintillator and the calibration of large arrays, Nucl. Instrum. Methods A 313 (1992) 367–372.